AD-A103 542 MASSACHUSETTS INST OF TECH LEXINGTON LINCOLN LAB F/G 20/5
ELECTROOPTICAL DEVICES.(U)
SEP 80 C E HURWITZ F19628-80-C-0002

UNCLASSIFIED ESD-TR-81-76 NL

END
DATE FILMED
10-81
DTIC

AD A103542

MASSACHUSETTS INSTITUTE OF TECHNOLOGY
LINCOLN LABORATORY

ELECTROOPTICAL DEVICES

SEMIANNUAL TECHNICAL SUMMARY REPORT TO THE ROME AIR DEVELOPMENT CENTER

1 APRIL – 30 SEPTEMBER 1980

ISSUED 8 JULY 1981

Approved for public release; distribution unlimited.

LEXINGTON MASSACHUSETTS

ABSTRACT

This report covers work carried out with support of the Rome Air Development Center during the period 1 April through 30 September 1980.

The gain spectra for TE polarization in a GaInAsP/InP laser have been measured as a function of DC bias current below laser threshold. The maximum net gain g_{max} is found to obey the relationship $g_{max} = (3.1 \times 10^{-2})(J_{nom}/\eta - 5.4 \times 10^{3})$, where J_{nom} is the nominal current density and η is the radiative quantum efficiency. The analysis of the results of the measurements leads to materials parameters which are important for optimizing laser design.

Improved versions of inverted-mesa n^+-InP/n-GaInAsP/n-InP/p^+-InP avalanche photodiode structures have been fabricated and characterized. Uniform avalanche gains of 700, dark-current densities of 3×10^{-6} A/cm^2 at a multiplication (M) of 10, and an excess noise factor of 3 (also at M = 10) have been achieved in diodes with wavelength cutoff at 1.25 μm.

A systematic study of the LPE growth of $Ga_xIn_{1-x}As_yP_{1-y}$ has been carried out over the entire range of layer compositions which are nearly lattice-matched to InP substrates. The results of the investigation enable the LPE-grown layer thickness to be calculated for various values of *step-cooling*, growth time, and composition.

A terraced surface morphology is found to be characteristic of heavily Zn-doped InP layers grown by LPE on substrates nominally oriented to (100). Noticeably smoother growth results if the substrates are oriented to a critical angle, which other workers have determined to be 2.6° off (100) in a ⟨110⟩ direction. For unintentionally doped and Sn-doped growths, the terraced morphology is not evident and the use of substrates oriented to the critical angle or those accurately oriented to (100) does not improve the morphology.

CONTENTS

ELECTROOPTICAL DEVICES

I. GAIN SPECTRA IN GaInAsP/InP PROTON-BOMBARDED STRIPE-GEOMETRY DH LASERS

A. INTRODUCTION

The spectral dependence of optical gain as a function of the level of injection of minority carriers is an important characteristic of semiconductor diode lasers. This dependence has been established both experimentally[1,2] and theoretically[3] for GaAs lasers with p-type, moderately doped ($\sim 4 \times 10^{17}$ cm^{-3}) active regions. In the GaInAsP alloy system, neither direct measurements nor fundamental calculations of this dependence have yet been reported, although an estimate[4] of the maximum gain as a function of injection level, based on the observed[5] dependence of laser threshold current density on active layer thickness, has been made for lasers emitting at 1.23-μm wavelength.

In this report, we describe the first measurements of gain spectra in GaInAsP lasers ($\lambda \sim 1.3$ μm). These measurements, which are similar to those made on GaAs lasers,[1,2] involve the Fabry-Perot resonances which occur in the spontaneous emission spectra of lasers. The results obtained can depend upon the properties of the device studied, if it contains inhomogeneities or other defects. Hence, it is important to select a high-quality device that is characterized as fully as possible. The data presented here are for one of our best devices, a proton-bombarded stripe-geometry laser[6] from a well-characterized wafer (wafer 4-4-78), numerous properties of which have been described in several earlier reports.[7-9]

Section B below reviews the characteristics, including growth and fabrication, of our test device and the wafer from which it comes. Section C describes the gain measurements and gives the results. In Sec. D, the results are discussed and compared with other data; and our conclusions are presented in Sec. E.

B. DEVICE CHARACTERISTICS

1. Growth and Fabrication

The GaInAsP/InP wafer (wafer 4-4-78) used in these experiments was prepared by liquid-phase-epitaxial growth of a double-heterostructure on a (100)-oriented, Sn-doped ($\sim 2 \times 10^{18}$ cm^{-3}) InP substrate. A Sn-doped ($\sim 2 \times 10^{18}$ cm^{-3}) buffer layer was first grown, followed by an undoped active layer 0.1 μm thick having a lattice-matched alloy composition with laser emission near 1.3-μm wavelength. This layer was not intentionally doped (but may become p-type because of Zn diffusion). A Zn-doped ($\sim 3 \times 10^{17}$ cm^{-3}) InP cap layer 3.8 μm thick was then grown. To assure good electrical contacts, the acceptor density near the surface of the top layer was increased to approximately 3×10^{18} cm^{-3} by means of a Zn diffusion. The sample was then masked and bombarded with a dose of 2×10^{15} cm^{-2} of 280-keV protons to provide 15-μm-wide stripe-geometry[6] devices over most of the wafer. The proton penetration depth was about 2.8 μm. A small portion of the wafer was reserved for broad-area, pulsed threshold measurements and was not exposed to the bombardment. Alloyed Au-Zn contacts to the cap layer and Au-Sn contacts to the substrate were used. Individual devices with cleaved mirrors and saw-cut walls were mounted on Cu heat sinks with In solder. Special techniques were used to assure that the

In layer between the device and the heat sink was as thin as possible. This appeared to minimize some of the problems[7,10-12] associated with the use of In solder.

2. Threshold Characteristics

In an earlier study on self-sustained pulsations,[9,13] pulsed threshold current densities ranging between 2 and 3.5 kA/cm^2 were measured for 58 stripe-geometry lasers from wafer 4-4-78, only 6 of which showed self-sustained pulsations. The threshold data are summarized in Fig. I-1, where the six abnormal devices are represented by triangular data points. As noted in Refs. 9 and 13, since these six devices are all approximately the same length, it is likely they are all from the same cleaved bar.

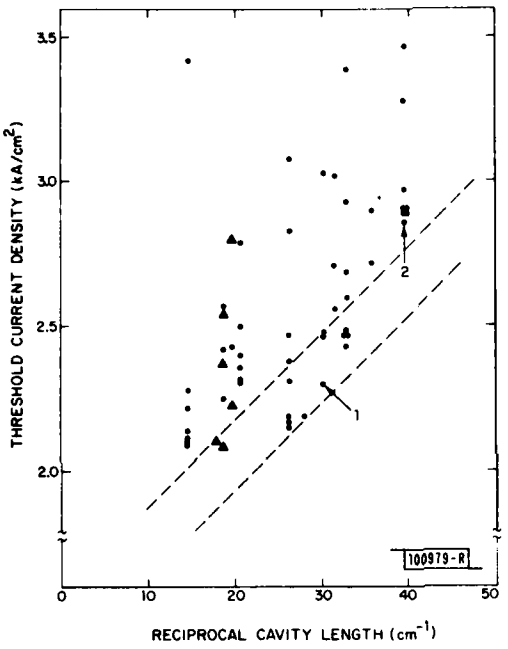

Fig. I-1. Pulsed threshold current density vs reciprocal cavity length for 58 lasers from wafer 4-4-78. Triangular data points indicate devices exhibiting sustained pulsations. Dashed lines are drawn with a slope determined by our gain-vs-current data and for loss coefficients differing by 10 cm^{-1}. Data points labeled 1 and 2, respectively, are for devices on which gain and pulse-response measurements were made.

The dashed straight lines in Fig. I-1 give the threshold vs reciprocal cavity length relationship deduced from the gain-measurement results to be described below. The lower line corresponds to a minimum loss coefficient, while the upper line was obtained for a loss coefficient 10 cm^{-1} higher than the minimum, as discussed below. The data points for about one-fourth of the devices fall between the two lines. The test device selected for the gain measurements, which is represented by the point labeled "1," has a reciprocal cavity length of 30.3 cm^{-1}.

The broad-area devices from wafer 4-4-78, which were 380 μm long, had an average threshold current density of 1.5 kA/cm^2, compared with 2.1 kA/cm^2 for the best stripe-geometry devices of that length. The 40-percent increase in threshold results from a reduction in quantum efficiency due to current spreading and lateral diffusion of injected carriers from the narrow stripe.[14] Between 10° and 70°C the pulsed threshold for the stripe-geometry lasers varied as exp [T/T$_o$], with T$_o$ = 67°C. (The maximum ambient temperature for CW operation of these

devices with outputs of several milliwatts per facet was just over 70°C.) Using the difference between the pulsed and CW thresholds to determine the temperature rise at the junctions, we have deduced thermal resistance values as low as 13°C/W, which is the value obtained for the device used for the gain measurements. Because of the low thermal resistance and low threshold currents, a number of packaged devices had CW thresholds at room temperature which were within a few percent of their pulsed values.

The spectra of the lasers usually showed several evenly spaced longitudinal modes near threshold. However, a single dominant mode was usually seen for currents 10 percent or more above threshold.

3. Confinement Factor

An important parameter used in interpreting the gain measurements is the confinement factor Γ, which gives the fraction of mode energy that is located within the active layer. The value of Γ can be calculated from the active layer thickness (d), using the slab waveguide approximation, if we know the refractive indices for InP (n_1) and GaInAsP (n_2). Nahory and Pollack[5] have plotted the refractive indices for InP and for lattice-matched alloys as a function of wavelength. At λ = 1.3 μm, their plot gives n_1 = 3.21 and n_2 = 3.51 for the alloy with bandgap corresponding to λ = 1.3 μm emission wavelength. For d = 0.1 μm, the value measured for our test device, the effective waveguide index calculated is $\bar{n}$ = 3.24 and the confinement factor is Γ = 0.2. In our analysis, this value of Γ will be used.

In order to provide a check on the values used for d, n_1, and n_2, we compared the far-field pattern measured for the test device with the theoretical one calculated with these values. This comparison is shown in Fig. I-2. Some asymmetry is seen in the experimental curve due to interference by the device package at 40°. The slight remaining discrepancy between theory and experiment can be removed if the value of $(n_2^2 - n_1^2)$ used in the calculation is increased by a few percent. Errors in measuring the far-field pattern or the active region thickness could also account for this discrepancy. The angle at full width, half-maximum is approximately 36°, in good agreement with the results of Itaya et al.,[15] but not with those of Henshall and Greene.[16]

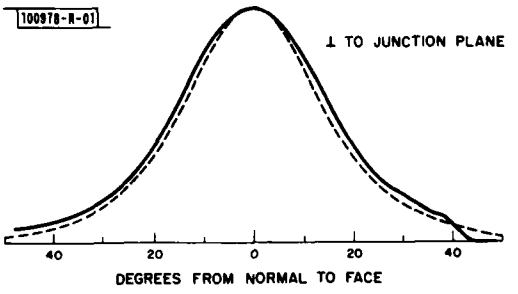

Fig. I-2. Far-field pattern of a device from wafer 4-4-78 in plane perpendicular to junction plane. Solid curve is experimental, and dashed curve was calculated for a 0.1-μm-thick active layer using refractive indices discussed in text. Agreement of two curves verifies that parameters used to determine confinement factor Γ are correct.

4. Carrier and Photon Lifetimes

The response of a laser to pulsed excitation can be used to determine the spontaneous lifetime of minority carriers τ_s and the photon lifetime τ_p, which is given by the relationship

$$\tau_p^{-1} = \frac{c\,[\alpha_i + (1/L)\,\ell n\,(1/R)]}{\bar{n}} \tag{I-1}$$

where c is the speed of light, α_i is the distributed loss coefficient of the cavity mode in which the laser operates, L is the cavity length, R is the mirror reflectivity, and $\bar{n}$ is the waveguide index. Pulse-response measurements for GaInAsP lasers have been reported by Akiba et al.[17] who used the following equations to analyze their data:

$$t_d = \tau_s\,\ell n[(I - I_o)/(I - I_{th})] \tag{I-2}$$

and

$$(2\pi f)^2 = I/(I_{th} - 1)/(\tau_s, \tau_p) \tag{I-3}$$

where t_d is the time delay between the onset of the pulse and the beginning of laser emission, I is the current, I_{th} is the threshold current, I_o is the DC bias current, and f is the frequency of the relaxation oscillation transient.

We have performed pulse-response measurements on a laser from wafer 4-4-78 that was mounted in a special package for high-speed experiments. This device, which was 254 μm long, is represented in Fig. I-1 by the point labeled "2." In their experiments, Akiba et al.[17] found that delays associated with space charge capacitance could be eliminated by applying values of DC bias I_o exceeding about 40 percent of the threshold value. We used similar DC bias levels and obtained the delay time results shown in Fig. I-3. The data are well fitted by a straight line passing through the origin. From Eq. (I-2), τ_s is the slope of this line, which is 1.2 ns. This value is smaller than those reported by Akiba et al.[17] However Oe et al.[18] found that values for τ_s in oxide-defined, stripe-geometry lasers depend on stripe width, and they obtained values comparable to ours for a similar stripe width. Recently, Hanamitsu et al.[19] attributed the reduced lifetime in narrow-stripe GaAlAs lasers to a number of factors including diffusion of carriers out of the stripe.

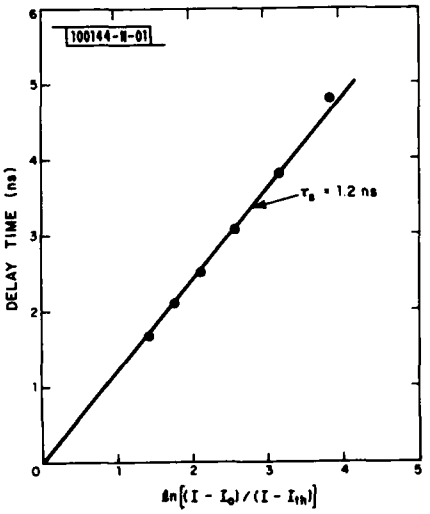

Fig. I-3. Delay time between applied current pulse and onset of stimulated emission plotted vs a factor in Eq. (I-2) of text. Solid line through points corresponds to relationship expected for a spontaneous lifetime of 1.2 ns.

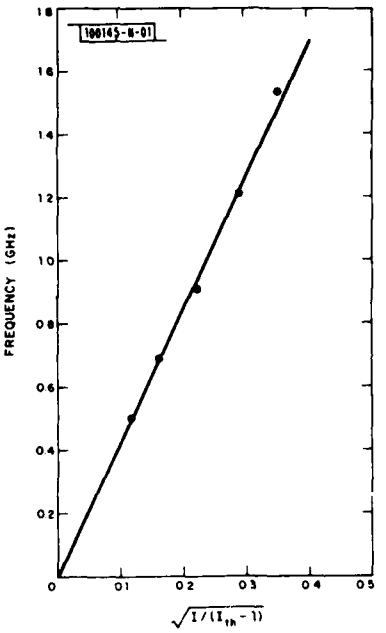

Fig. I-4. Frequency of relaxation oscillation transient as a function of pulsed current amplitude I and threshold current I_{th}. Slope of line is used to determine that $\tau_p \approx 1.2$ ps. [See Eq. (I-1).]

The measured frequency of the relaxation oscillation transient is plotted vs the square root of $I/(I_{th} - 1)$ in Fig. I-4. Again, a straight line passing through the origin is obtained, as predicted by Eq. (I-3). The good agreement with Eq. (I-3) is somewhat unexpected, since the equation is based on a rather simple model of the rate equations and applies only in the small-signal regime, as pointed out by Akiba et al.[17] With $\tau_s = 1.2$ ns, the slope of the line in Fig. I-4 yields a value of 1.2 ps for τ_p and Eq. (I-1) then gives 93 cm^{-1} for $\alpha_2 + (1/L_2)\,\ell n\,(1/R)$, where the subscript 2 refers to the device used for the pulse-response measurements. If we use

$$R \approx \left(\frac{\bar{n} - 1}{\bar{n} + 1}\right)^2 = 0.28$$

mirror losses become $(1/L_2)\,\ell n\,(1/R) \approx 49$ cm^{-1}, yielding $\alpha_2 \approx 44$ cm^{-1}.

By means of a procedure described in Sec. IV, we have used this value of α_2 in determining loss coefficients for the other devices of Fig. I-1. For the best of these, $\alpha_i \approx 30$ cm^{-1} – a value comparable to the loss in GaAs lasers with a similar active layer thickness (Ref. 20). There are two contributions to the cavity loss coefficient: free-carrier absorption, and scattering due to waveguide wall roughness. For confining layers with low carrier concentrations and for a small confinement factor, the free-carrier loss may be small. However, scattering can become important for thin active layers.[20] In general, the smaller the confinement factor and the larger the index difference between the active and confining layers, the larger the scattering losses. Compared with GaAs lasers with 30% Al in the confining layers, GaInAsP layers emitting at $\lambda = 1.3$ μm have both smaller confinement factors and larger index differences for the same active layer thickness. However, scattering may be somewhat reduced at the longer wavelength due to other dependences of scattering on wavelength.[21]

C. GAIN MEASUREMENTS

To determine the gain of our test device, we measured its spontaneous emission spectrum at a number of bias currents. In making such measurements on GaAs lasers, liquid-nitrogen-cooled photomultiplier tubes can be used as detectors. There is no comparably sensitive detector available at 1.3-μm wavelength and, hence, low-noise measurements are more difficult. We used a PbS photoconductor, a 450-Hz mechanical chopper, and a lock-in amplifier to achieve good signal-to-noise ratios. Using a procedure described by Hakki and Paoli,[1,2] we focused a magnified image (X6) of the output mirror of the laser onto the spectrometer slits, which were comparable to or smaller than the magnified stripe width. This procedure discriminates against collection of unguided spontaneous emission.

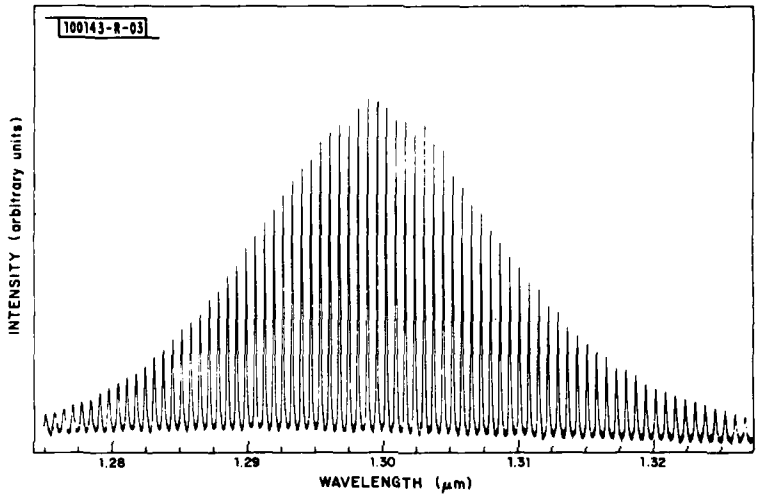

Fig. I-5. Spontaneous emission spectrum for TE polarization at 101 mA. Structure is due to longitudinal Fabry-Perot modes or resonances of cavity below threshold (117 mA).

Figure I-5 is the spontaneous emission spectrum for TE polarization taken at a DC bias level of 101 mA for the test device, whose CW threshold current is 117 mA. The spectral resolution is 0.5 Å. If we denote the relative intensity of the emission at one of the maxima of the Fabry-Perot resonances seen in Fig. I-5 by P^+ and the intensity at a neighboring minimum by P^-, then as shown by Hakki and Paoli[1,2] the net gain experienced by the guided light (at a wavelength between the wavelengths at the maximum and minimum) is given by

$$-\alpha - \frac{1}{L} \ln \frac{1}{R} = \frac{1}{L} \ln \left[\frac{(P^+/P^-)^{1/2} - 1}{(P^+/P^-)^{1/2} + 1} \right] \qquad \text{(I-4)}$$

where $-\alpha = \Gamma g - \alpha_i$, in which g is the gain coefficient in the active layer.

Spectra similar to the one shown in Fig. I-5 were also taken at 60, 70, 80, 90, and 111 mA. We did not analyze data for larger currents (near threshold and above), where the spectral peaks become very narrow and difficult to resolve and the minima approach the background noise level. Also, signals for TM polarization were too low for analysis.

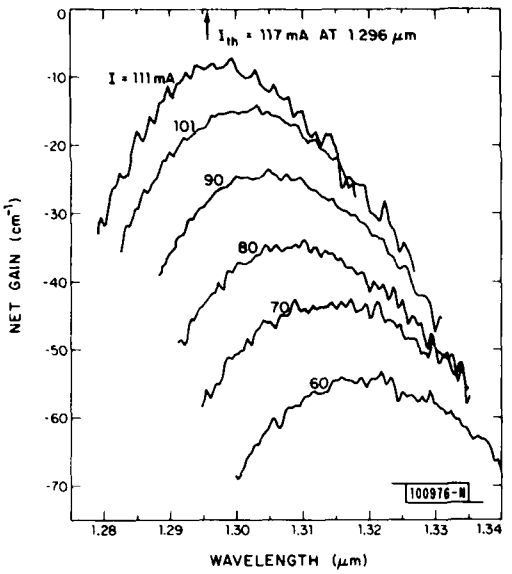

Fig. I-6. Net gain vs wavelength calculated from spontaneous spectrum at each bias current labeled in milliamperes.

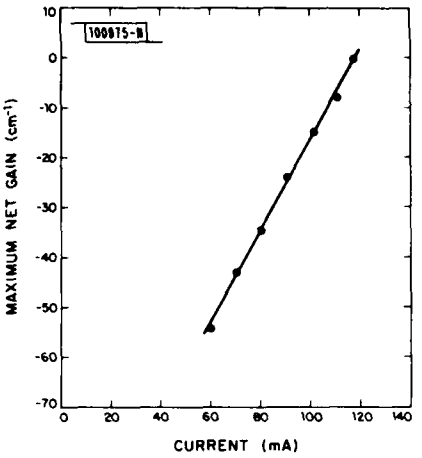

Fig. I-7. Maximum net gain as a function of wavelength plotted vs bias current.

In Fig. I-6 the net gain at each bias current, calculated from the right-hand side of Eq. (I-4), is plotted *vs* wavelength. The shift of the maximum gain to shorter wavelengths with increased current is expected because of band filling at the higher injection levels. Finally, In Fig. I-7 we have plotted the maximum value of the net gain at each current vs the current. The point at threshold (117 mA) was not obtained from spectral data, but rather was obtained by noting that net gain at threshold is equal to zero by definition. The straight line drawn through the data points fits the equations

$$\Gamma g_{max} - \alpha_1 - \frac{1}{L_1} \ln \frac{1}{R} = -105 + 897\, I \qquad \text{(I-5a)}$$

$$= -105 + 0.044\, J \qquad \text{(I-5b)}$$

where I is the current in amperes, J is the current density in A/cm^2, and the subscript 1 refers to the device used for the gain measurements.

D. DISCUSSION

In order to compare our results with the results for GaAs lasers, we need to express g_{max} in the form[20]

$$g_{max} = \beta(J_{nom} - J_o) \qquad \text{(I-6)}$$

where β and J_o are parameters to be determined, and the nominal current density J_{nom} is given by $\eta J/d$, with η the quantum efficiency below threshold. For our devices $\eta = \eta_r/1.4$, where η_r is the radiative efficiency of the active layer and the factor of 1.4 represents the loss of efficiency due to current spreading and lateral diffusion in the stripe-geometry device as mentioned in Sec. B-2.

In evaluating β and J_o from the experimental relationship given by Eq. (I-5), it is necessary to use the numerical value of α_1. We have obtained this value from the measured loss coefficient ($\alpha_2 = 44\ cm^{-1}$) of the device used for the pulse-response measurements. To do so, we add the quantity $[\alpha_1 - \alpha_i + (1/L_1)\,\ell n(1/R) - (1/L)\,\ell n(1/R)]$, where α_i and L are variable, to both sides of Eq. (I-5b):

$$\Gamma g_{max} - \alpha_i - \frac{1}{L}\,\ell n\frac{1}{R} = -105 + 0.044\,J + \alpha_1 - \alpha_i + \frac{1}{L_1}\,\ell n\frac{1}{R} - \frac{1}{L}\,\ell n\frac{1}{R} \quad . \tag{I-7}$$

At $J = J_{th}$, Eq. (I-7) equals zero. Hence,

$$J_{th} = \frac{1}{0.044}\left[105 + (\alpha_i - \alpha_1) - \frac{1}{L_1}\,\ell n\frac{1}{R} + \frac{1}{L}\,\ell n\frac{1}{R}\right] \quad . \tag{I-8}$$

Substituting $1/L_1 = 30.3\ cm^{-1}$ and $\ell n(1/R) = 1.26$, we obtain

$$J_{th} = 1.5 \times 10^3 + 23(\alpha_i - \alpha_1) + 29\,\frac{1}{L} \quad . \tag{I-9}$$

Substituting for device 2 the values $J_{th} = 2.87 \times 10^3\ A/cm^3$, $\alpha_i = 44\ cm^{-1}$, and $L = 254\ \mu m$, we obtain $\alpha_1 = 34\ cm^{-1}$. With α_1 set equal to this value in Eq. (I-9), the upper and lower dashed lines in Fig. I-1 were obtained for $\alpha_i = 30\ cm^{-1}$ and $40\ cm^{-1}$, respectively.*

In terms of J_{nom} (expressed in A/cm^2-μm), Eq. (I-5b) becomes

$$g_{max} = 0.044\,\frac{dJ_{nom}}{\eta\Gamma} - \frac{1}{\Gamma}\left(105 - \alpha_1 - \frac{1}{L_1}\,\ell n\frac{1}{R}\right) \quad . \tag{I-10}$$

The values of the parameters in Eq. (I-10) have been discussed in detail above. Using those values [$d = 0.1\ \mu m$, $\eta = \eta_r/1.4$, $\Gamma = 0.2$, $\alpha_1 = 34\ cm^{-1}$, and $(1/L_1)\,\ell n(1/R) = 38\ cm^{-1}$], we obtain

$$g_{max} = \frac{3.1 \times 10^{-2}}{\eta_r}\,(J_{nom} - \eta_r\, 5.4 \times 10^3). \tag{I-11}$$

For a fixed wavelength near the lasing wavelength of their GaAs laser, Hakki and Paoli[2] found that

$$g = 5.45 \times 10^{-2}(J_{nom} - 4 \times 10^3) \tag{I-12}$$

which agrees well with Stern's[3] calculated maximum gain coefficient

$$g_{max} = 5.0 \times 10^{-2}(J_{nom} - 4.5 \times 10^3) \quad . \tag{I-13}$$

If we assume that $0.5 \leqslant \eta_r \leqslant 1$ (see Refs. 22 and 23), the numerical values for β and J_o obtained from Eq. (I-11) are $6.2 \times 10^{-2} \geqslant \beta \geqslant 3.1 \times 10^{-2}$ cm-μm/A and $2.7 \times 10^3 \leqslant J_o \leqslant 5.4 \times 10^3\ A/cm^2$-$\mu m$, similar to the values in GaAs.

---

* For $\alpha_i = \alpha_1 = 34\ cm^{-1}$, Eq. (I-9) gives a line that would pass slightly above point 1 in Fig. I-1, because the CW threshold given by Eq. (I-9) was measured to be 2-percent larger for the test device than the pulsed threshold, which is plotted in Fig. I-1.

When the linear relationship of Eq. (I-6) applies, at large values of d the confinement factor Γ approaches unity and J_{th}/d approaches a constant value given by[20]

$$J_{th}/d = J_o/\eta_r + \frac{[\alpha_i + (1/L)\,\ell n(1/R)]}{\beta\eta_r} \quad . \tag{I-14}$$

Using our experimental values of J_o/η_r and $\beta\eta_r$ and assuming $[\alpha_i + (1/L)\,\ell n(1/R)] \sim 50\ cm^{-1}$ for large d, where scattering losses are low, we obtain $J_{th}/d \sim 7 \times 10^3$ A/cm^2-μm. This value is larger than most experimental values[5,15,16] for devices with d > 0.5 μm. However, the data on which this value is based were all taken for very large values of J_{nom} ($J_{nom}/\eta \geq 10^4$ A/cm^2-μm) because Γ is small and α_i is large in the test device. Since devices with large d would have larger Γ and smaller α_i, they would operate at lower values of J_{nom} where the linear relationship of Eq. (I-6) may not apply. Stern's[3] calculations for GaAs deviate from linearity below about 5×10^3 A/cm^2-μm. For GaAs lasers with thick active layers (d > 0.5 μm), threshold data appear to be slightly better fit[20] using a dependence of the form $g_{max} = \beta(J_{nom} - J_o)^2$. The effect of deviation from the linear relationship could be stronger in GaInAsP. Another factor which may significantly reduce threshold in GaInAsP devices with large d is an increase in the apparent carrier lifetime due to reabsorption of the spontaneous emission on subsequent passes through the active layer, as predicted by Liau in Sec. II of this report.

Our results in Eq. (I-11) also differ from the estimates of Botez,[4] who deduced $\beta\eta_r \sim 20 \times 10^{-2}$ cm-μm/A and $J_o \sim \eta_r\ 1.75 \times 10^3$ A/cm^2-μm. Again, however, his estimates are based on data for small J_{nom} and large d.

E. CONCLUSIONS

We have made the first direct measurement of gain spectra as a function of current in GaInAsP lasers. The results show a linear dependence of maximum gain on current, as expected for the high-gain, high-injection-level regime that occurs in lasers with narrow active layers. The data are well represented by a relationship of the form $g_{max} = \beta(J_{nom} - J_o)$. Since the test device and the wafer from which it comes have been well characterized, reasonable estimates could be made for all the parameters needed in the analysis except the radiative quantum efficiency. If we assume that $0.5 \leq \eta_r \leq 1$, the values obtained for β and J_o lie within 65 percent of the values obtained for those quantities in GaAs.

Extrapolation of our results to devices with thick active layers yields calculated threshold current densities that are larger than the experimental values. While part of the discrepancy may be due to accumulated errors in estimating the parameters used in the extrapolation, it seems likely that other explanations are also needed. Two reasonable possibilities are that the linear gain-current relationship observed here does not hold at lower nominal current densities and that the apparent carrier lifetime (and, hence, quantum efficiency) is larger in devices with thick active layers due to reabsorption of the spontaneous emission on subsequent passes through the active layer (see Sec. II). Further work to measure gain in devices with thick active layers is under way.

J. N. Walpole J. J. Hsieh
T. A. Lind J. P. Donnelly

II. THE RECYCLING OF SPONTANEOUS PHOTONS IN GaInAsP/InP DOUBLE-HETEROSTRUCTURE LASERS

A theoretical analysis has been carried out which reveals the significance of the transparency of the InP substrate to the spontaneous light emitted by the GaInAsP active layer in GaInAsP/InP double-heterostructure (DH) lasers. Because of the metallic contacts and the large difference of the refractive indices between InP and air, the spontaneously emitted photons will bounce around within the device and have a large probability of being reabsorbed by the active layer (via band-to-band transitions). This reabsorption of spontaneous light could have significant effects in lowering the threshold current density in semiconductor lasers. The idea of photon recycling was considered previously by Stern and Woodall[24] with reference to GaAs/GaAlAs lasers. However, the effect would be expected to be negligibly small because of the large absorption in the GaAs substrate at the lasing wavelength.

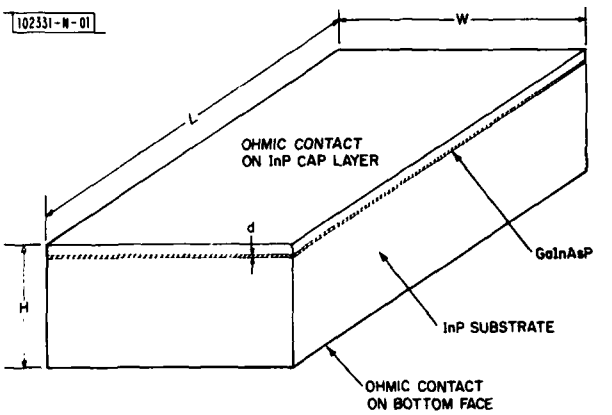

Fig. II-1. Schematic drawing of broad-area GaInAsP/InP DH laser diode used in present calculation. Shaded region is GaInAsP active layer. Top and bottom faces (L × W) are ohmic contacts.

Figure II-1 shows a schematic drawing of a broad-area GaInAsP/InP DH laser diode. Most of the spontaneous light emitted from the active layer will be reflected by the two metallic ohmic contacts (top and bottom in Fig. II-1) and the sidewalls and be confined to the device volume. We will therefore treat the spontaneous light as a photon gas filling the whole device. For simplicity, we ignore the absorption at the metallic contacts. There are then three major processes which contribute to the consumption of the spontaneous photons, namely: (a) transmission through the sidewalls of the device, (b) free-carrier absorption in the InP substrate and cladding layers, and (c) reabsorption (band-to-band) in the active layer. (The total free-carrier absorption in the active layer is small relative to the substrate and cladding layers, since the active layer is generally much thinner.)

Only those photons impinging upon the sidewall within an angle <20° (critical angle) of the surface normal can be transmitted into the air.[25] The average transmission probability for photons within this angle per bounce is ~70 percent. Therefore, the number of photons

transmitted into the air per unit time R_t is given by

$$R_t \cong NA \frac{c}{\bar{n}} \times \frac{\Omega}{4\pi} \times 0.70 \qquad \text{(II-1)}$$

where N is the photon density (per unit volume) in the device, $A \equiv 2$ (LH + WH) is the total area of the sidewalls (cf. Fig. II-1), $c/\bar{n}$ is the speed of light in InP (with $\bar{n}$ being the refractive index of InP), and Ω is the solid angle within which transmission is possible. It can easily be shown that $\Omega/4\pi = 0.0302$.

The number of photons absorbed by the free carriers in InP per unit time R_a is given by

$$R_a \cong NV \frac{c}{\bar{n}} \alpha_{InP} \qquad \text{(II-2)}$$

where V = LWH is the total volume of the device, and α_{InP} is the average free-carrier absorption coefficient of the InP substrate and cladding layers. The number of photons reabsorbed in the active layer per unit time R_r is given by

$$R_r \cong NV \frac{c}{\bar{n}} \frac{d}{H} \bar{\alpha}_Q \qquad \text{(II-3)}$$

where d is the active layer thickness (in general, $d \ll H$), and $\bar{\alpha}_Q$ is the average band-to-band absorption coefficient in the active layer.

The fraction f of the spontaneous photons which is reabsorbed by the active layer is given by $f \equiv R_r/(R_r + R_a + R_t)$. By combining Eqs. (II-1) through (II-3), we get

$$f = \frac{\bar{\alpha}_Q d/H}{\bar{\alpha}_Q \frac{d}{H} + \alpha_{InP} + \frac{0.042(L + W)}{LW}} \cdot \qquad \text{(II-4)}$$

The magnitude of f will be of great importance in the laser characteristics. Using Eq. (II-4), we have evaluated f as a function of active layer thickness d for typical device dimensions and several possible values of α_{InP} and $\bar{\alpha}_Q$. The results are shown in Fig. II-2.

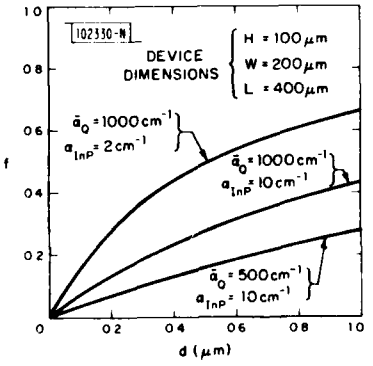

Fig. II-2. Fraction of spontaneous photons reabsorbed by GaInAsP active layer in broad-area GaInAsP/InP DH laser (Fig. II-1), obtained by present calculation [Eq. (II-4)].

The immediate effect of the reabsorption of the spontaneous photons is an effective lengthening of the radiative carrier lifetime and the consequent lowering of the laser threshold current density. To see this, we suppose that the radiative carrier lifetime without the reabsorption

is τ_r. With the reabsorption, the effective radiative carrier lifetime is now

$$\tau_r' = \frac{\tau_r}{1-f} \quad . \tag{II-5}$$

The ratio of the threshold current densities with and without the reabsorption is then given by

$$\frac{J_{th}' \text{ (with reabsorption)}}{J_{th} \text{ (without reabsorption)}} = \frac{\tau}{\tau'} \tag{II-6}$$

where $\tau' \equiv \tau_{nr}\tau_r'/(\tau_{nr} + \tau_r')$ and $\tau \equiv \tau_{nr}\tau_r/(\tau_{nr} + \tau_r)$ are total carrier lifetimes with and without the reabsorption, respectively. (τ_{nr} is the nonradiative carrier lifetime.) After some rearranging, the lowering of the threshold current density can be expressed as

$$\frac{J_{th} - J_{th}'}{J_{th}} = \eta f \tag{II-7}$$

where $\eta \equiv \tau_{nr}/(\tau_{nr} + \tau_r)$ is the internal quantum efficiency of the laser without the reabsorption. Note that η will be a limiting factor in the threshold-current lowering.

In Eq. (II-3) an average absorption coefficient $\bar{\alpha}_Q$ has been used for the band-to-band reabsorption of the spontaneous photons. The value of $\bar{\alpha}_Q$ will depend on the functional dependence of the absorption coefficient on energy, which in turn depends on the band structure and electron-hole injection.[26] Those spontaneous photons with energies in the gain region (the lower energy portion of the spontaneous spectrum)[27] will have a net probability of being amplified, rather than being absorbed, when passing through the active layer. These photons will not only make a negative contribution to f, but probably will also contribute to the noise in the laser emission. However, with gain $\leq 100\ cm^{-1}$ these photons will more likely be absorbed in the InP or be transmitted through the device sidewalls.

The present calculations show that, for the general case of broad-area GaInAsP/InP lasers, appreciable amounts of reabsorption of the spontaneous photons and lowering of the laser threshold current density can occur [Fig. II-2 and Eq. (II-7)]. Based on the same calculations, improved results can be expected if the device structure is optimized to minimize the free-carrier absorption in InP and the transmission loss through the sidewalls and/or to enhance the absorption in the active layer. These can be achieved by using low substrate doping, a thin substrate, Au-coated sidewalls (except for the laser emission region), and a thicker active layer, etc. In addition to the broad-area lasers, the same concept can be applied to other laser structures. Among the stripe-geometry lasers, the buried-heterostructure and strip-buried-heterostructure lasers are most pertinent, because there is no unpumped region of the GaInAsP layer which will contribute to the loss of spontaneous light. The same principles can also be applied to the GaAs/GaAlAs lasers if the highly absorbing GaAs substrates can be removed or optically isolated from the finished devices.

The reabsorption of the spontaneous photons is also likely to affect the temperature dependence of the threshold current. Generally speaking, the increase of threshold current accompanying an increase in temperature is mainly due to an increase in the energy spread of the injected carriers. The result is that the maximum gain is lowered and more carriers are wasted in generating spontaneous emission.[26] This will also cause an increase in $\bar{\alpha}_Q$ and a consequent

increase in f. Reabsorption of spontaneous photons will thus have a tendency to reduce the temperature dependence of the threshold current and to increase the reliability of the device.

Z. L. Liau
J. N. Walpole

III. LOW DARK-CURRENT, HIGH-GAIN GaInAsP/InP AVALANCHE PHOTODETECTORS

Further improvements have been achieved in the performance of inverted-mesa GaInAsP/InP APDs similar to those described in a previous report (see p. 7 in Ref. 9). The present structure, shown in the inset of Fig. III-1, differs from the earlier inverted-mesa APD structures in that a 1 μm thick cap layer of Sn-doped n^+-InP ($N_D = 2 \times 10^{18}$ cm^{-3}) has been added and the surface passivation has been improved. The surface passivation, which was found to be critical to attainment of reproducibly low dark currents ($\sim 3 \times 10^{-6}$ A/cm^2 at 0.9 V_B), was accomplished by application of a DuPont polyimide film (5 to 8 μm thick) directly over the freshly etched mesas.[28,29] The film was patterned using standard photolithographic techniques and cured by baking at 200 °C for 1 hr. Devices so passivated were found to be highly stable in normal room atmosphere and under sustained high values of bias voltage.

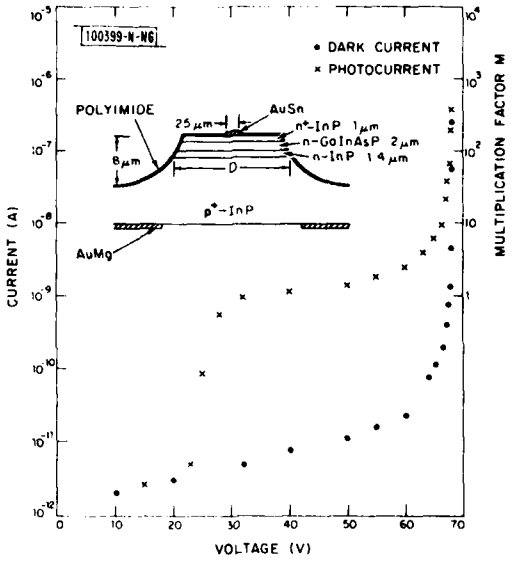

Fig. III-1. I-V characteristics of GaInAsP/InP APD with D = 76.2 μm. Photoresponse was taken at DC and 200 Hz using chopped 1.15-μm light and at frequencies ranging from 1 kHz to 25 MHz using modulated output of 1.21-μm GaInAsP laser. Multiplication factor was measured with 1 nA of primary photocurrent. (Inset: Device structure; device diameter D varied from 64 to 152 μm.)

Typical reverse I-V characteristics with and without light are shown in Fig. III-1. The photocurrent measurements were performed at DC and 200 Hz by illuminating the device with chopped 1.15-μm light from a He-Ne laser, and at frequencies from 1 kHz to 25 MHz by using the modulated output of a 1.21-μm GaInAsP laser. The multiplication vs bias was independent of frequency over this range. Pulse-response measurements indicate that the frequency response extends beyond 2 GHz, as discussed below. The onset of the photoresponse beginning

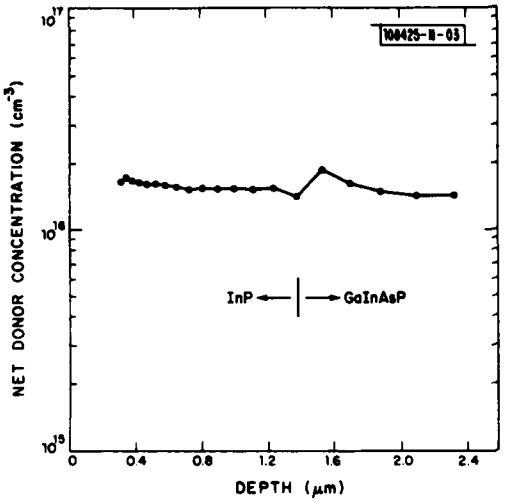

Fig. III-2. Net carrier concentration profile obtained from C-V measurements. Discontinuity occurs at n-InP/n-GaInAsP heterojunction.

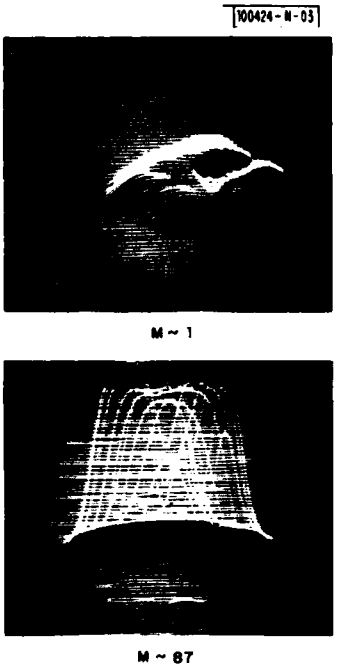

Fig. III-3. Scanned photoresponse with 1.15-μm light incident from front.

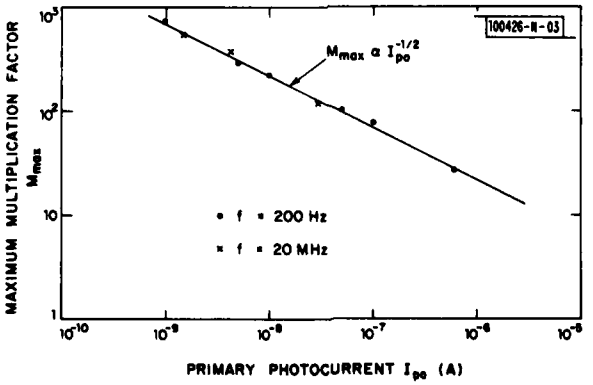

Fig. III-4. Maximum achievable multiplication M_{max} as a function of primary photocurrent I_{po}.

at about 23 V corresponds to the punch-through of the depletion region from the InP into the GaInAsP. Above this voltage the photogenerated holes, which at low bias are confined to the GaInAsP by the valence-band barrier of the heterojunction, are swept by the electric field into the InP and then collected at the junction.[30,31] The values of the multiplication were calculated by assuming a gain of unity at 32 V, a voltage just above the step and at the beginning of the nearly flat region in the photoresponse-vs-bias curve. The fact that the onset of photoresponse corresponds to the penetration of the depletion region into the GaInAsP is confirmed by the results of C-V measurements, as shown in Fig. III-2. The inflection in the computed carrier concentration profile occurs at a voltage corresponding to a depletion depth equal to the n-InP layer thickness.

The photoresponse obtained by scanning the device from the front is shown in Fig. III-3 at a bias of 32 V (M = 1) and near the breakdown voltage (M = 87). Except for the fact that there was no obstruction by the probe wire, scans of the back side of the devices yielded identical results. The difference in gain from the front and back observed in the early structures (see p. 7 in Ref. 9) was eliminated by the addition of the n^+-InP cap layer. The response is quite uniform over the entire area for gains up to 87, which was the maximum obtainable at the relatively high photocurrent (100 nA) required for the measurement. The maximum attainable multiplication factor decreased with increasing primary photocurrent over the range of 1 nA to 1 μA, in good agreement with the gain saturation model of Melchior and Lynch,[32] as shown in Fig. III-4. This effect appeared to be independent of frequency. The maximum measured multiplication, obtained for a primary photocurrent of 1 nA, was ~700.

In Fig. III-5, for the same device, the measured dark current at a given bias voltage has been plotted as a function of the photocurrent multiplication factor at that same bias. At low values of multiplication (covering the bias range from about 20 to 60 V), the current rises rapidly as the depletion region spreads into the GaInAsP from the wider-gap InP and the dark current (presumably due to bulk space charge generation) increases and begins to be multiplied. Over the range of multiplication from approximately 2 to 50 (corresponding to a bias range of ~60 to 67 V)

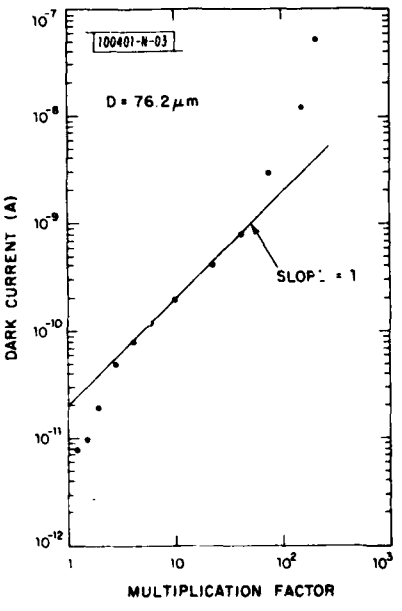

Fig. III-5. Dark current vs multiplication.

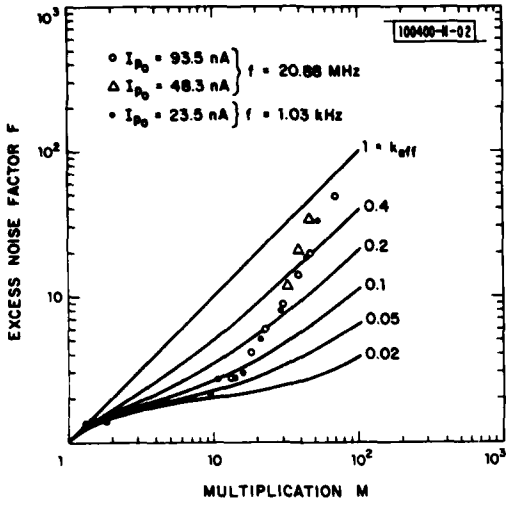

Fig. III-6. Experimental excess noise factor vs multiplication for several primary photocurrents and frequencies. Solid curves were calculated from theory of McIntyre.[34,35]

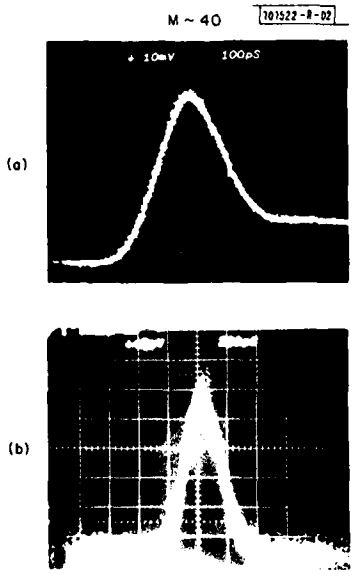

Fig. III-7. Photoresponse to 200-ps pulse from 1.06-μm Nd:YAG laser. (a) Light incident from front; (b) light incident from back.

the dark current is proportional to the multiplication, indicating that over this range the dominant component of the dark current is bulk space charge generation current which is being multiplied by the avalanche process. At larger values of multiplication (i.e., biases above 67 V) the dark current rises more rapidly than the multiplication, indicating that the electric field in the GaInAsP itself has increased to the point that the anomalous leakage currents (possibly due to tunneling[33]), observed in conventional GaInAsP p-n junction devices, become dominant.

Noise measurements as a function of multiplication were made at several frequencies from 200 Hz to 25 MHz and for varying levels of illumination, incident from both the front and the back of the detector. A sensitive spectrum analyzer and low-noise transimpedance amplifiers were employed. The excess current $\overline{i_n^2} = 2eBI_pM^2F$, where B is the bandwidth and I_p is the primary photocurrent, was calculated from the measured values of noise added by the incident light and the concurrently measured multiplication. The data are plotted in Fig. III-6 as a function of multiplication. The solid curves were calculated from the theoretical expression of McIntyre[34,35]: $F(M) = M\{1 - [(1 - k)(1 - M)^2]/M^2\}$, where k is the ratio of electron-to-hole ionization coefficients α/β under the assumption that α/β is independent of electric field. When the electric field dependence of α/β is included, k may be replaced by an effective value k_{eff} (see Refs. 34 and 35). The measured values of F were found to be independent of photocurrent, frequency, and direction of illumination. They also indicate that $\alpha/\beta < 1$, in qualitative agreement with results obtained in InP (see Ref. 36). (The photo-generated carriers swept into the InP and then multiplied are purely holes.) As evident from Fig. III-6, low values of F, consistent with a k_{eff} of 0.02 to 0.1, are found for $M < 10$. For larger values of multiplication, F increases considerably more rapidly than expected; the reason for this result is not presently known. Multiplication in the GaInAsP, for which recent measurements[37] indicate that $\alpha/\beta > 1$, can apparently be ruled out since the maximum field there is less than that at which multiplication is observed in APDs with the p-n junction in GaInAsP of the same composition. Similar behavior has been observed[38] in Si APDs, but it appears to be dependent on the specific device structure.

Response-time measurements were performed using 200-ps-wide pulses of 1.06-μm radiation from a mode-locked Nd:YAG laser. The pulse response with a primary photocurrent of 600 nA and a gain of 40 for light incident from either the front or the back is shown in Fig. III-7(a-b). The measured risetime of ~160 ps is limited by the laser. The "back porch" evident in the waveform when illuminated from the front is due to the carriers which are generated in the undepleted GaInAsP and must diffuse to the high-field region. With illumination from the back, nearly all the carriers are generated in the depleted GaInAsP and no slow component of the response is observed. Similar response could be achieved from the front by tailoring the device parameters so that the GaInAsP is fully depleted. From the results obtained from response measurements,[39] pulsewidths of <80 ps can be expected on conventional inverted-mesa GaInAsP/InP APDs, whose response characteristics should not differ substantially from the present devices.

The quantum efficiency of the GaInAsP/InP photodiodes measured from the front was 50 percent, a value which is somewhat lower than the reflection-limited maximum of 70 percent because of carrier recombination in the undepleted region of the GaInAsP. Higher quantum efficiency with light incident from the front can be obtained by making the thickness and carrier concentration of the GaInAsP such that the depletion region extends to within a diffusion length of the n-GaInAsP/n^+-InP interface. For back illumination, the quantum efficiency is low

because of free-carrier absorption in the heavily doped p-type substrate. Thinning of the wafer or the use of more lightly doped p^+-InP substrates will be required to achieve high quantum efficiencies in this mode.

The GaInAsP/InP APDs described here are considerably more sensitive than any other competitive device reported earlier, in spite of the fact that further optimization is still possible and that at high values of multiplication they exhibit noise levels which are higher than predicted. Work is presently under way to determine the cause of this rise in excess noise factor as well as to extend the sensitivity range of these structures to ~1.5 μm.

V. Diadiuk C. E. Hurwitz
S. H. Groves G. W. Iseler

IV. THICKNESS OF LPE $Ga_xIn_{1-x}As_yP_{1-y}$ LAYERS NEARLY LATTICE-MATCHED TO (100)-InP SUBSTRATES

Precise thickness control in the LPE growth of quaternary layers is required in order to realize the full potential of $Ga_xIn_{1-x}As_yP_{1-y}$/InP optoelectronic devices. In the extreme case of InP (i.e., $x = y = 0$), the growth thickness has been studied as a function of growth-solution composition, temperature, and time.[40] However, only a few scattered data have been reported for the quaternary.[41-44] In this work, a systematic study has been carried out over the entire range of quaternary layer compositions which are nearly lattice-matched to the InP substrates ($|\Delta a/a| \leq 0.3$ percent).

Ten different quaternary growth-solution compositions have been used in the present work. (The growth solutions and samples were the same as those used in a previous study of the growth-temperature dependence of LPE GaInAsP/InP lattice mismatch.[45]) First, the liquidus temperature T_ℓ (at which the solution and small crystallites were equilibrated) was determined to an accuracy of ±0.5°C for each growth-solution composition. The ten T_ℓ's were found to exhibit a range of temperature between 639.5° and 650.5°C. Then, by using the step-cooling technique,[40] several LPE growth runs were carried out for each growth solution. A constant growth temperature T_g was used for each LPE run. The amount of step-cooling, $\Delta(\equiv T_\ell - T_g)$, was normally between 4° and 11°C; the growth time was between 0.5 and 10 min. These growth conditions resulted in quaternary layers of 0.6- to 4.5-μm thickness, which were measured by using an optical microscope.

The observed layer thickness d, as a function of step cooling Δ and growth time t, showed good agreement with the following relationship derived for the diffusion-limited growth mechanism[40]

$$d = C\Delta \cdot t^{1/2} \qquad \text{(IV-1)}$$

where the coefficient C is a "material constant" and is presumably a relatively slow-varying function of temperature.[40] The value of C for $Ga_{0.5}In_{0.5}As$ (i.e., the extreme case of $y = 1$) is obtained from the data of Fig. IV-1. The slope of the line is the coefficient C, according to Eq. (IV-1). Figure IV-2 shows the experimental C-values thus determined for the entire range of quaternary compositions. The y-values in Fig. IV-2 were obtained by using an empirical relationship between the quaternary wavelength λ_Q and composition.[46] A single variable y is used to specify the quaternary composition because of the relationship between x and y imposed by the lattice-matching condition.[46]

Figure IV-2 shows a nearly constant C-value for 0.92 μm ($\equiv \lambda_{InP}$) $\leq \lambda_Q \lesssim$ 1.3 μm. Moreover, this C-value is in good agreement with the value obtained for the growth of InP layers.[40] These observations suggest that (similar to the InP growth) the phosphorous diffusion in the solution is the rate-limiting step in these growths. This agrees with the fact that phosphorus has a much larger distribution coefficient (and, therefore, will be depleted over a much longer distance from the growth front) than the other three components of the quaternary. An analogous argument may also be applied to the rise in C-value in the extreme long-wavelength region in Fig. IV-2 in which phosphorus is not present. (That the C-value for $y = 1$ is nearly one order of magnitude larger than that for $0 \leq y \leq 0.6$ agrees with the observation that gallium has a distribution coefficient one order of magnitude smaller than that of phosphorus.[47])

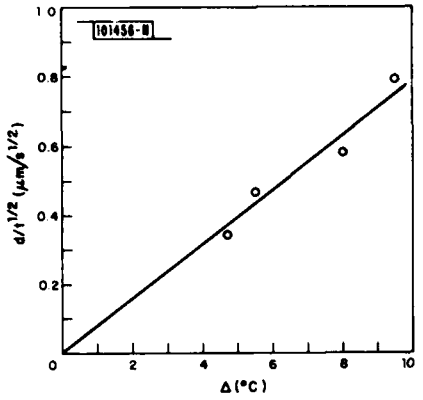

Fig. IV-1. Relationship between thickness d, growth time t, and amount of step-cooling Δ in the LPE growth of $Ga_{0.5}In_{0.5}As$ layers on (100) InP.

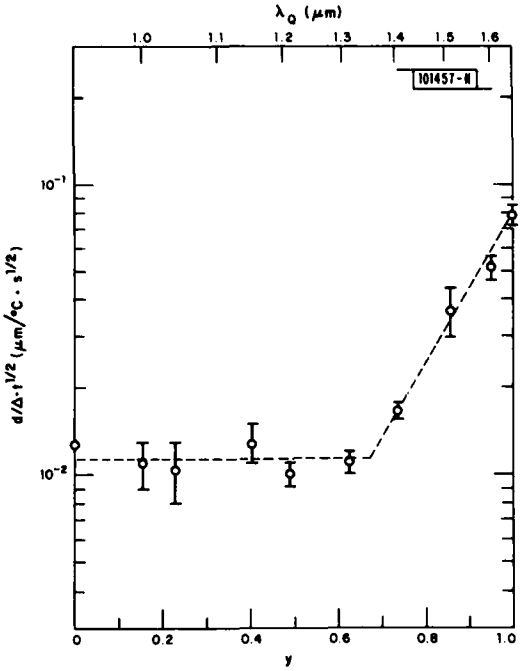

Fig. IV-2. Dependence of coefficient C (as defined in $d = C\Delta \cdot t^{1/2}$) on $Ga_xIn_{1-x}As_yP_{1-y}$ composition in LPE growth of quaternary layers on (100) InP.

In conclusion, we have carried out a study on the thickness of LPE $Ga_xIn_{1-x}As_yP_{1-y}$ layers as a function of growth temperature, time, and composition. Despite the system's complexity, the results were combined into a more unified picture. We believe that the present results are also very useful in the preparation of heterostructures for optoelectronic devices.

Z. L. Liau

V. LPE SURFACE MORPHOLOGY OF InP(Zn)

A terraced surface morphology sometimes occurs with liquid-phase-epitaxial (LPE) growth on substrates misoriented from a low-index plane. The terraces usually consist of relatively wide treads of the low-index plane and narrow risers at a small angle Θ to the low-index plane. Θ does not change with the amount of misorientation, and, as a result, terrace-free growth occurs both for substrates oriented on the low-index plane and at an angle Θ from the low-index plane, designated as the critical orientation.[48,49] In the case of InP LPE-grown layers on InP substrates of nominal (100) orientation, $\Theta \simeq 2.6°$ toward $\langle 100 \rangle$ (Ref. 50).

We have found that the terraced morphology is characteristic of InP growth in some, but not all, situations. Terraced growth occurs for layers that are heavily doped with Zn ($N_A \geq 5 \times 10^{17}$ cm^{-3}). A photomicrograph of growth with $N_A \simeq 1 \times 10^{18}$ cm^{-3} on a nominally oriented (100) substrate is shown in Fig. V-1(a), and the terrace morphology is evident. Growth from the same solution but using a substrate nominally oriented 2.6° off the (100) in a $\langle 110 \rangle$ direction gives a smoother and markedly different morphology as shown in Fig. V-1(b). The closely spaced terraces of Fig. V-1(b) are what would be expected if the substrate were oriented at slightly less than Θ from the low-index plane.

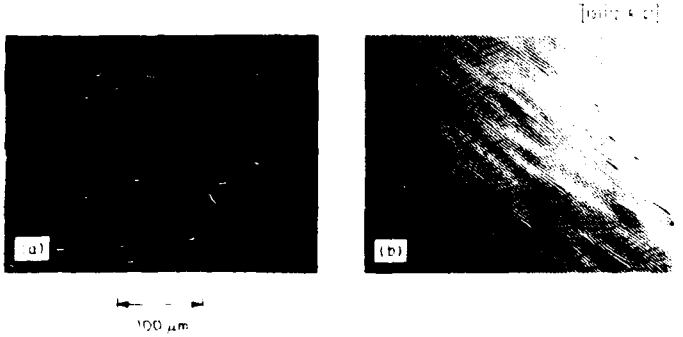

Fig. V-1. Photomicrographs of growth from a Zn-doped solution (giving $N_A \simeq 1 \times 10^{18}$ cm^{-3}) with (a) a substrate of nominal (100) orientation and (b) a substrate nominally oriented at 2.6° off (100).

For not intentionally doped and Sn-doped growth, there is only slight evidence of terraced growth. Little or no improvement in smoothness results in these cases from using substrates that are either accurately oriented to (100) (within 0.1°) or oriented 2.6° off (100). Our growths are usually made within the temperature range of 630° to 700°C; they are initiated with a supercooling of 5° to 10°C and are grown at a cooling rate of 0° to 0.7°C/M. The results for the undoped and Sn-doped growths seem to suggest that, under these conditions, morphology defects are not related to the terracing phenomena. This is apparently similar to the case of GaAs(Sn) where even small amounts of supercooling tend to eliminate terracing.[51]

From these preliminary results, it would seem for the case of LPE InP(Zn) growth that efforts to orient substrates accurately to (100) or nominally to the critical orientation should result in improved morphology. There are two minor disadvantages to using the 2.6°-off

orientation (critical orientation): (a) if a meltback with an indium solution is used, the etched surface is not as smooth as for nominally oriented (100) substrates; and (b) if too large a deviation from the (100) occurs, nucleation problems with resulting island growth are seen. This is most likely to be a problem with substrates that have edge rounding due to etching.

S. H. Groves
M. C. Plonko

REFERENCES

1. B. W. Hakki and T. L. Paoli, J. Appl. Phys. 44, 4113 (1973).
2. _____, J. Appl. Phys. 46, 1299 (1975).
3. F. Stern, J. Appl. Phys. 47, 5382 (1976).
4. D. Botez, Appl. Phys. Lett. 35, 57 (1979).
5. R. E. Nahory and M. A. Pollack, Electron. Lett. 14, 727 (1978).
6. J. J. Hsieh, J. A. Rossi, and J. P. Donnelly, Appl. Phys. Lett. 28, 709 (1976), DDC AD-A028550/2.
7. Semiannual Technical Summary on Electrooptical Devices, Lincoln Laboratory, M.I.T. (30 September 1978), p. 1, DDC AD-A069091/7.
8. Ibid. (31 March 1979), p. 1, DDC AD-A077153/5.
9. Ibid. (30 September 1979), p. 1, DDC AD-A084410/0.
10. Y. Horikoshi, H. Saito, and M. Kawashima, Jpn. J. Appl. Phys. 18, 1623 (1979).
11. R. G. Plumb, A. R. Goodwin, and R. S. Baulcomb, IEE J. Solid-State Electron Dev. 3, 206 (1979).
12. K. Fujiwara, H. Imai, T. Fujiwara, K. Hari, and M. Takusagwa, Appl. Phys. Lett. 35, 861 (1979).
13. J. N. Walpole, T. A. Lind, J. J. Hsieh, and A. G. Foyt, Appl. Phys. Lett. 36, 240 (1980), also see Ref. 9.
14. H. C. Casey, Jr. and M. B. Panish, Heterostructure Lasers, Part B (Academic Press, New York, 1978), pp. 217-224.
15. Y. Itaya, Y. Suematsu, S. Katayama, K. Kishino, and S. Arai, Jpn. J. Appl. Phys. 18, 1795 (1979).
16. G. D. Henshall and P. D. Greene, IEE J. Solid-State Electron Dev. 3, 174 (1979).
17. S. Akiba, Y. Itaya, K. Sakai, T. Yamamoto, and Y. Suematsu, Trans. IECE Jpn. E61, 124 (1978).
18. K. Oe, S. Ando, and K. Sugiyama, J. Appl. Phys. 51, 43 (1980).
19. K. Hanamitsu, H. Ishikawa, and H. Nishi, IEEE J. Quantum Electron. QE-16, 596 (1980).
20. H. C. Casey, Jr. and M. B. Panish, op. cit., pp. 180-187.
21. D. Marcuse, Light Transmission Optics (Van Nostrand Reinhold, New York, 1972), pp. 368-379.
22. R. E. Nahory, M. A. Pollack, and J. C. DeWinter, Electron. Lett. 15, 695 (1979).
23. G. H. B. Thompson and G. D. Henshall, Electron. Lett. 16, 42 (1980).
24. F. Stern and J. M. Woodall, J. Appl. Phys. 45, 3904 (1974).
25. H. Kressel and J. K. Butler, Semiconductor Lasers and Heterojunction LEDs (Academic Press, New York, 1977), p. 135.
26. H. C. Casey, Jr. and M. B. Panish, Heterostructure Lasers, Part A, Ch. 3 (Academic Press, New York, 1978).
27. See, for example, H. Kressel and J. K. Butler, op. cit., p. 110.
28. Semiannual Technical Summary on Electrooptical Devices, Lincoln Laboratory, M.I.T. (31 March 1980), p. 5, DDC AD-A092699.
29. V. Diadiuk, C. A. Armiento, S. H. Groves, and C. E. Hurwitz, Electron. Device Lett. EDL-1, 177 (1980).
30. K. Nishida, K. Taguchi, and Y. Matsumoto, Appl. Phys. Lett. 35, 251 (1979).

31. K. Taguchi, Y. Matsumoto, and K. Nishida, Electron. Lett. 15, 453 (1979).

32. H. Melchior and W. T. Lynch, IEEE Trans. Electron Devices ED-13, 829 (1966).

33. S. R. Forrest, M. DiDomenico, Jr., R. G. Smith, and H. J. Stocker, Appl. Phys. Lett. 36, 580 (1980).

34. R. J. McIntyre, IEEE Trans. Electron Devices ED-13, 164 (1966).

35. _____, IEEE Trans. Electron Devices ED-19, 703 (1972).

36. C. A. Armiento, S. H. Groves, and C. E. Hurwitz, Appl. Phys. Lett. 35, 333 (1979), DDC AD-A076467/0.

37. M. Ito, T. Kaneda, K. Nakajima, Y. Toyoma, and T. Kotani, Electron. Lett. 14, 418 (1978).

38. S. Takamiya, A. Kondo, and K. Shirahata, Tech. Digest Mon. Meeting Opto- and Quantum Electron. (Japan), Paper 1974-8.

39. S. R. Chinn and W. K. Zwicker, Appl. Phys. Lett. 34, 847 (1979), DDC AD-A076426/6.

40. J. J. Hsieh, Chapter 2 in Gallium Arsenide and Related Compounds (St. Louis) 1976, L. F. Eastman, Ed. (The Institute of Physics, Bristol and London, 1977), p. 74, DDC AD-A046988/2.

41. K. Sakai, S. Akiba, T. Yamamoto, Jpn. J. Appl. Phys. 16, 2043 (1977).

42. Y. Itaya, Y. Suematsu, S. Katayama, K. Kishino, and S. Arai, Jpn. J. Appl. Phys. 18, 1795 (1979).

43. S. Akiba, K. Sakai, Y. Matsushima, and G. E. Stillman, Jpn. J. Appl. Phys. 19, L79 (1980).

44. M. Feng, L. W. Cook, M. M. Tashima, and G. E. Stillman, J. Electron. Mater. 9, 241 (1980).

45. Semiannual Technical Summary on Electrooptical Devices, Lincoln Laboratory, M.I.T. (31 March 1980), p. 13, DDC AD-A092699.

46. R. E. Nahory, M. A. Pollack, W. D. Johnston, Jr., and R. L. Barns, Appl. Phys. Lett. 33, 659 (1978).

47. M. Feng, T. H. Windhorn, M. M. Tashima, and G. E. Stillman, Appl. Phys. Lett. 32, 758 (1978).

48. D. L. Rode, Phys. Status Solidi A 32, 425 (1975).

49. S. L. Rode, R. W. Wagner, and N. E. Schumaker, Appl. Phys. Lett. 30, 75 (1977).

50. R. Messham and A. Majerfeld, Abstract 21st Electronics Materials Conf., Boulder, Colorado, June 1979, p. 31.

51. N. Toyoda, M. Mihara, and T. Hara, Jpn. J. Appl. Phys. 18, 2207 (1979).

UNCLASSIFIED

SECURITY CLASSIFICATION OF THIS PAGE (When Data Entered)

REPORT DOCUMENTATION PAGE

READ INSTRUCTIONS BEFORE COMPLETING FORM

1. REPORT NUMBER: ESD-TR-81-76	2. GOVT ACCESSION NO.
3. RECIPIENT'S CATALOG NUMBER	
4. TITLE (and Subtitle): Electrooptical Devices	5. TYPE OF REPORT & PERIOD COVERED: Semiannual Technical Summary, 1 April - 30 September 1980
6. PERFORMING ORG. REPORT NUMBER	
7. AUTHOR(s): Charles E. Hurwitz	8. CONTRACT OR GRANT NUMBER(s): F19628-80-C-0002
9. PERFORMING ORGANIZATION NAME AND ADDRESS: Lincoln Laboratory, M.I.T., P.O. Box 73, Lexington, MA 02173	10. PROGRAM ELEMENT, PROJECT, TASK AREA & WORK UNIT NUMBERS: Program Element Nos. 62702F and 61102F; Project Nos. 2306 and 4600
11. CONTROLLING OFFICE NAME AND ADDRESS: Rome Air Development Center, Griffiss AFB, NY 13440	12. REPORT DATE: 30 September 1980
	13. NUMBER OF PAGES: 34
14. MONITORING AGENCY NAME & ADDRESS (if different from Controlling Office): Electronic Systems Division, Hanscom AFB, Bedford, MA 01731	15. SECURITY CLASS. (of this report): Unclassified
	15a. DECLASSIFICATION DOWNGRADING SCHEDULE

16. DISTRIBUTION STATEMENT (of this Report)

Approved for public release; distribution unlimited.

17. DISTRIBUTION STATEMENT (of the abstract entered in Block 20, if different from Report)

18. SUPPLEMENTARY NOTES

None

19. KEY WORDS (Continue on reverse side if necessary and identify by block number)

electrooptical devices
avalanche photodiodes
proton bombardment
double-heterostructure
ion implantation
GaInAsP/InP lasers

20. ABSTRACT (Continue on reverse side if necessary and identify by block number)

This report covers work carried out with support of the Rome Air Development Center during the period 1 April through 30 September 1980.

The gain spectra for TE polarization in a GaInAsP/InP laser have been measured as a function of DC bias current below laser threshold. The maximum net gain g_{max} is found to obey the relationship $g_{max} = (3.1 \times 10^{-2})(J_{nom}/\eta - 5.4 \times 10^{3})$, where J_{nom} is the nominal current density and η is the radiative quantum efficiency. The analysis of the results of the measurements leads to materials parameters which are important for optimizing laser design.

DD FORM 1 JAN 73 1473 EDITION OF 1 NOV 65 IS OBSOLETE

UNCLASSIFIED

SECURITY CLASSIFICATION OF THIS PAGE (When Data Entered)

221657

20. ABSTRACT (Continued)

Improved versions of inverted-mesa n^+-InP/n-GaInAsP/n-InP/p^+-InP avalanche photodiode structures have been fabricated and characterized. Uniform avalanche gains of 700, dark-current densities of 3×10^{-6} A/cm^2 at a multiplication (M) of 10, and an excess noise factor of 3 (also at M = 10) have been achieved in diodes with wavelength cutoff at 1.25 μm.

A systematic study of the LPE growth of $Ga_xIn_{1-x}As_yP_{1-y}$ has been carried out over the entire range of layer compositions which are nearly lattice-matched to InP substrates. The results of the investigation enable the LPE-grown layer thickness to be calculated for various values of step-cooling, growth time, and composition.

A terraced surface morphology is found to be characteristic of heavily Zn-doped InP layers grown by LPE on substrates nominally oriented to (100). Noticeably smoother growth results if the substrates are oriented to a critical angle, which other workers have determined to be 2.6° off (100) in a ⟨110⟩ direction. For unintentionally doped and Sn-doped growths, the terraced morphology is not evident and the use of substrates oriented to the critical angle or those accurately oriented to (100) does not improve the morphology.

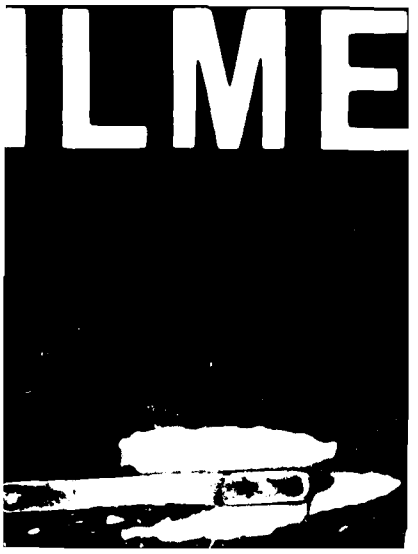
ILME